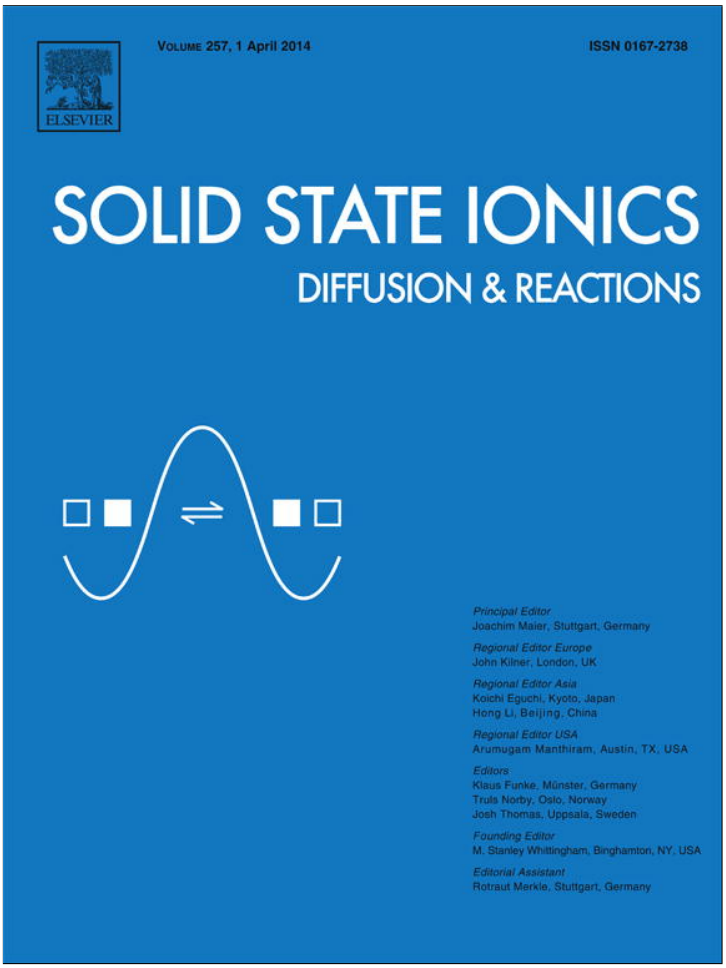

Solid State Ionics 257 (2014) 67–74

Contents lists available at ScienceDirect

Solid State Ionics

journal homepage: www.elsevier.com/locate/ssi

Influence of structural arrangement of R_2O_2 slabs of layered cuprates on high-temperature properties important for application in IT-SOFC

G.N. Mazo [a], S.M. Kazakov [a], L.M. Kolchina [a], S.Ya. Istomin [a,*], E.V. Antipov [a], N.V. Lyskov [b], M.Z. Galin [b], L.S. Leonova [b], Yu.S. Fedotov [c], S.I. Bredikhin [c], Yi Liu [d], G. Svensson [d], Z. Shen [d]

[a] Department of Chemistry, Moscow State University, Leninskie Gory, Moscow 119991, Russia
[b] Institute of Problems of Chemical Physics RAS, Academician Semenov av. 1, Chernogolovka, Moscow District 142432, Russia
[c] Institute of Solid State Physics RAS, 2 Academician Ossipyan str., Chernogolovka, Moscow District 142432, Russia
[d] Department of Materials and Environmental Chemistry, Stockholm University, Stockholm S-10691, Sweden

ARTICLE INFO

Article history:
Received 11 November 2013
Received in revised form 14 January 2014
Accepted 24 January 2014
Available online 14 February 2014

Keywords:
Layered cuprates
Thermal expansion
Oxygen diffusion
Cathode materials
High-temperature conductivity

ABSTRACT

Layered cuprates $Pr_{2-x}Sr_xCuO_{4-\delta}$ with T* (x = 0.3, 0.4) and T (x = 1.0, 1.3) structures were prepared in air at 1273–1373 K. Oxygen content (4 − δ) of the as-prepared phases decreases from 3.96 (x = 0.3) and 3.98 (x = 0.4) to 3.69 (x = 1.0) and 3.49 (x = 1.3), respectively, as determined by chemical titration. Dilatometry measurements revealed non-linear expansion with low- and high-temperature regions occurring due to thermogravimetrically detected oxygen loss. Different expansion behaviors in low- and high-temperature regions of T- and T*-phases are attributed to various distributions of oxygen vacancies in their crystal structures. Both x = 0.4 and 1.0 ceramic samples exhibit lower conductivity values at high temperatures in comparison with undoped Pr_2CuO_4. The temperature dependences of the electrical conductivity at variable oxygen partial pressure (p_{O_2} = 10^{-4}–0.21 atm) reveal different mechanisms of the holes generation in x = 0.4 and 1.0 compounds. The tracer diffusion coefficient of oxygen (D_T) in $Pr_{1.6}Sr_{0.4}CuO_{3.98}$ determined by isotopic exchange depth profile (IEDP) technique using secondary ion mass spectrometry (SIMS) is in the range 6.7×10^{-10}–5.7×10^{-8} cm^2/s at 973–1223 K. Obtained values are in between those for La_2CuO_4 and Pr_2CuO_4 with pure rock-salt and fluorite slabs in the crystal structure, respectively. This shows the importance of rock-salt slabs for high oxygen conductivity in R_2MO_4 oxides.

1. Introduction

A major target in the development of solid-oxide fuel cells (SOFCs) is the decrease of their operating temperature down to 550–750 °C (intermediate temperature SOFC or IT-SOFC) [1]. For this purpose standard cathode material based on Sr doped $LaMnO_3$ (LSM) should be replaced by oxygen-deficient perovskites with 3d-elements like Fe, Co, Ni or Cu. These compounds may show improved oxide-ion conductivity at elevated temperatures and, therefore, due to the changes in the mechanism of oxygen reduction in comparison with LSM, are much more effective for the application in IT-SOFC [2]. Recently, layered cuprates R_2CuO_4, R = La–Gd, have attracted attention as cathode materials in IT-SOFC. La_2CuO_4 combines high values of oxygen diffusion (D_T) and surface exchange (k) coefficients (~1×10^{-8} cm^2 s^{-1} and ~1×10^{-6} cm s^{-1} at 973 K, respectively [3]) with a low thermal expansion coefficient (TEC) value of 12.3 ppm K^{-1}. However, it exhibits nearly temperature-independent low electrical conductivity ~15 S/cm at 1273 K [3,5]. La_2CuO_4 is the only one phase among rare-earth cuprates that crystallizes in the so-called T-type structure (Fig. 1a). It may be considered to be the first member of Ruddlesden–Popper series $A_{n+1}B_nO_{3n+1}$, where copper has axially distorted octahedral coordination. This structure may also be considered as an intergrowth of perovskite and rock-salt La_2O_2 slabs. Tetrahedral voids in La_2O_2 slabs of T-phase may participate in the diffusion of oxide-ions as it was revealed by molecular dynamic (MD) studies [6]. Other rare-earth cuprates R_2CuO_4 with R = Pr–Gd have T′-structure with square coordination of copper (Fig. 1b). This structure type may be considered as an intergrowth between perovskite and fluorite R_2O_2 slabs. In T′-structure there are empty octahedral voids participating in the diffusion of oxide ions [7]. Compressed fluorite slab makes the diffusion of oxygen in cuprates with T′-structure much slower in comparison with T-type. For example, oxygen tracer diffusion coefficient in Pr_2CuO_4 (7.2×10^{-13} cm^2 s^{-1} at 973 K) is by nearly five orders of magnitude lower in comparison with La_2CuO_4 and the mechanism of oxygen reduction on Pr_2CuO_4 resembles that one of LSM [8]. However, layered cuprates with T′-structure have a number of advantages as cathode materials in IT-SOFC. This especially concerns Pr_2CuO_4 having high total electrical conductivity > 100 S/cm at 1173 K and low linear TEC of 11.8 ppm K^{-1} [9].

In the present work, we report on the study of thermal expansion behavior, high-temperature crystal structure and electrical conductivity of $Pr_{2-x}Sr_xCuO_{4-\delta}$, $0.0 < x \leq 1.5$. In this system three phases with different crystal structures T′- (x = 0.0), T- (x = 1.0) and T*-phases (x = 0.4) were found [10]. In the structure of T*-phase an ordering of smaller Pr and larger Sr cations over two crystallographic positions

* Corresponding author. Tel.: +7 495 9393490; fax: +7 495 9394788.
E-mail address: istomin@icr.chem.msu.ru (S.Y. Istomin).

0167-2738/$ – see front matter © 2014 Elsevier B.V. All rights reserved.
http://dx.doi.org/10.1016/j.ssi.2014.01.039

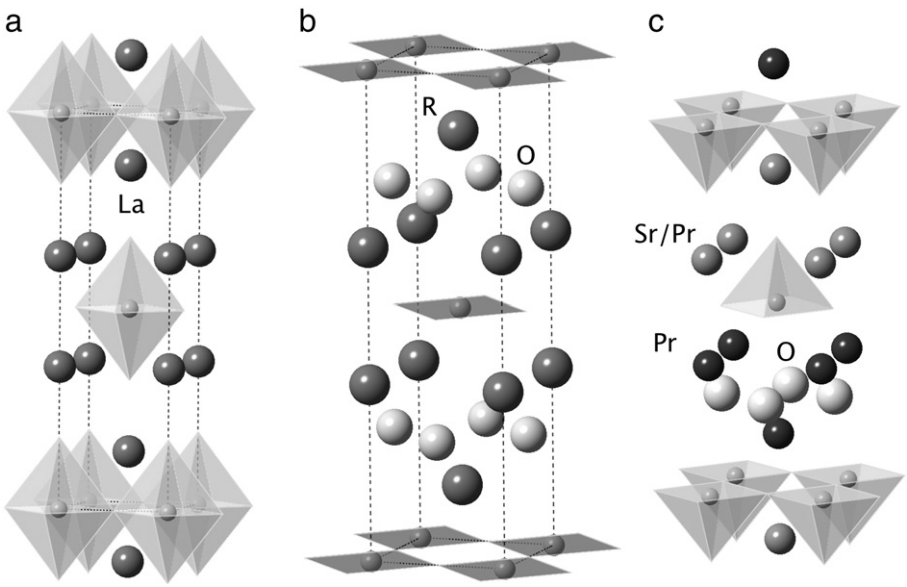

Fig. 1. The crystal structures of T- (La_2CuO_4, a), T′- (R_2CuO_4, R = Pr–Gd, b) and T*- ($Pr_{1.6}Sr_{0.4}CuO_{3.98}$, c) phases. For T*-phase there is a preferential for large cations (Sr) to the position with CN = 9 (rock-salt slab) and for smaller (Pr) to the position with CN = 8 (fluorite slab).

leads to the presence of both rock-salt and fluorite structure slabs (see Fig. 1c). In order to confirm the importance of the rock-salt slabs in the crystal structure of layered oxides for fast oxygen diffusion, we have studied oxygen tracer diffusion in $Pr_{1.6}Sr_{0.4}CuO_{3.98}$ by isotopic exchange depth profile (IEDP) technique using secondary ion mass spectrometry (SIMS).

2. Experimental

Samples of $Pr_{2-x}Sr_xCuO_{4-\delta}$, x = 0.0, 0.1, 0.3, 0.4, 0.6, 0.8, 1.0, 1.3 and 1.5 were prepared by reacting of intimately mixed stoichiometric amounts of CuO, $SrCO_3$ and Pr_6O_{11} at 1273–1373 K for 20 h in air. Phase purity of the compounds was checked by means of X-ray powder diffraction (XRPD) data recorded in a Huber G670 Guinier diffractometer ($CuK_{\alpha1}$ radiation, image foil detector). High-temperature X-ray powder diffraction (HT XRPD) data were collected in air using Bruker D8-Advance diffractometer ($CuK_{\alpha1}$ radiation, LynxEye PSD) in reflection mode equipped with high-temperature camera XRK-900 (Anton Paar). Unit cell parameters of the cuprates at high-temperatures were obtained from the refinement of their crystal structures by Rietveld method using TOPAS-3 program package.

Oxygen content of the single-phase samples was determined by iodometric titration. Procedure was performed in two stages. At the first stage about 30 mg of the sample was dissolved in 20 mL of water containing 5 drops of concentrated HCl and boiled in air for 10 min. After that 20 mL of 20% KI water solution was added. Chemical reaction may be represented as follows:

$$2Cu^{2+} + 4I^- \rightarrow 2CuI + I_2.$$

The released elemental iodine was titrated with a standard $Na_2S_2O_3$ solution with starch added as an indicator. At the second stage about 30 mg of the sample was dissolved in 10 mL of 20% KI water solution containing 5 drops of concentrated HCl under stirring in closed flask. In this case chemical reaction may be described by the equation:

$$2Cu^{2+} + Cu^{3+} + 7I^- \rightarrow 3CuI + 2I_2.$$

The released iodine was titrated by the procedure described above. The amount of Cu^{3+} and corresponding oxygen content of the samples was calculated from the difference of these two titrations.

Netzsch 402C dilatometer operated in air (298–1173 K, 10 K/min) was used for the thermal expansion coefficient measurements. For this purpose powders of cuprates were pressed into pellets (8 mm in diameter and 5.0–5.5 mm in height) and sintered at 1343 K.

Thermogravimetric (TG) studies were performed in artificial air (20% O_2(g), 80% Ar(g)) and Ar(g) at 298–1173 K with a heating rate of 10 K/min using Netzsch STA 449C thermoanalyser.

Electrical conductivity measurements of the ceramic samples were performed by a conventional four-point DC technique in the temperature range of 373–1173 K at the oxygen partial pressures of 10^{-4}–0.21 atm. The sintered samples have a typical shape of a rectangular bar (approximate dimension of 20 mm × 8 mm × 3 mm) with relative density of ~90%. Platinum ink painted on lateral surface of the sample acted as a current collector and as oxygen electrodes. Platinum wires pressed into bulk of the samples were used as potentional electrodes (a distance between Pt-wires was about 10 mm). DC conductivity was measured using a P-30 potentiostate/galvanostate (Elins Ltd, Russia) in cyclic voltamperometry (CVA) mode in the voltage range from −50 mV to 50 mV at the voltage scan rate of 20 mV/s. The resulting specific resistivity was recalculated from the slopes of CVA curves taking into account the current collector area and the distance between potentional electrodes. The oxygen partial pressure was monitored by means of zirconia sensor. The temperature of the sample was measured by a Pt–Pt/Rh thermocouple positioned close to the sample with an accuracy of ±1 K.

Dense ceramic samples of $Pr_{1.6}Sr_{0.4}CuO_{3.98}$ for SIMS study were prepared by spark plasma sintering (SPS). 2.0–2.4 g of powder was filled into a graphite die with an inner diameter of 12 mm. The temperature was measured with an optical pyrometer focused on the surface of the graphite die and automatically regulated from 873 to 1273 K at a heating rate of 50 K/min. The temperature of 873 K was reached via a preset heating program by 4 min. The holding time was set to 3 min at the final temperature. A constant uniaxial pressure of 50 MPa was applied during the whole sintering period. After sintering, a surface layer (about 0.5 mm) of the ceramic sample was removed by polishing with sandpaper and ultrasonically cleaned in acetone to remove polish residues. Phase purity of the ceramic sample was checked by XRD. Density of the ceramic samples of $Pr_{1.6}Sr_{0.4}CuO_{3.98}$, as determined by pycnometry, was 91.2% relative to the calculated X-ray density.

Prior to ^{18}O exchange annealing, samples were held at 973, 1073, 1123 and 1173 K in air of natural isotopic abundance for a period of time approximately one order of magnitude longer than the tracer

annealing time. This was carried out to ensure that the material was in chemical equilibrium at the desired temperature and oxygen partial pressure (in this study all annealings were carried out at nominal oxygen partial pressure of 0.2 atm). The air was then removed, and labeled oxygen (95% enriched $^{18}O_2$) introduced. Annealing times were 90 min at 973 K, 120 min at 1073 K, 60 min at 1173 K and 25 min at 1223 K. The ^{18}O penetration profiles were determined on a TOF-SIMS 5 instrument operated in depth profiling mode, with a 45° incidence 25 keV Bi^+ primary ion beam; the crater depth was measured after the SIMS analysis by surface profilometry (Taylor–Hobson Talystep).

3. Results and discussion

3.1. XRPD and TG studies

Single-phase samples of $Pr_{2-x}Sr_xCuO_{4-\delta}$ were prepared with x = 0.0, 0.3, 0.4, 1.0 and 1.3. Reflections in their XRPD patterns were fully indexed with unit cell parameters given in Table 1. The obtained values of the unit cell parameters of x = 0.0, 0.4 and 1.0 samples correspond to the literature data [10]. Among the prepared compounds only Pr_2CuO_4 crystallizes in T′-structure (Fig. 1b), while high substitution level of praseodymium by the larger strontium cations (x = 1.0 and 1.3) leads to the formation of T-phases (Fig. 1a). Intermediate compositions (x = 0.3 and 0.4) have T*-phase structure (Fig. 1c). Oxygen stoichiometry of the prepared samples determined by iodometric titration is presented in Table 1. Oxygen content of undoped praseodymium cuprate corresponds to stoichiometric one within e.s.d., i.e. $Pr_2CuO_{4.02\pm0.02}$. For x = 0.3 and 0.4 samples it is only slightly lower than stoichiometric: $Pr_{1.7}Sr_{0.3}CuO_{3.96\pm0.02}$ and $Pr_{1.6}Sr_{0.4}CuO_{3.98\pm0.02}$. Compounds with T-structure have high amount of oxygen vacancies corresponding to chemical formulae $PrSrCuO_{3.69\pm0.02}$ and $Pr_{0.7}Sr_{1.3}CuO_{3.49\pm0.02}$. Multiphase samples were obtained for compositions with x = 0.1, 0.6, 0.8 and 1.5. This corresponds to literature data for PrO_x–SrO–CuO system [11,12].

Thermogravimetric (TG) analysis in air of x = 0.0, 0.4 and 1.0 samples revealed that oxygen content in x = 0.4 and 1.0 samples decreases with temperature (Fig. 2). For Pr_2CuO_4 no appreciable weight loss was detected. XRPD data of the samples after the TG experiments in air and Ar confirmed phase stability of cuprates. For both x = 0.4 and 1.0 samples the decrease of weight in air starts at ~673 K, however, for the former one it is less pronounced although it accelerates at ~973 K (Fig. 2a). The different temperature dependences of the oxygen content may be explained considering both oxidation state of copper and the peculiarities of the crystal structures of the studied cuprates. In the crystal structure of T′-phase (Pr_2CuO_4) Cu^{2+} has square coordination (coordination number (CN) = 4) only. This hinders further the decrease of its CN and oxygen atoms from Pr_2O_2 fluorite slab are also tightly linked with Pr^{3+}. In the T*-structure copper cations are in tetragonal pyramidal coordination (CN = 5). This allows decreasing of oxygen content by the formation of oxygen vacancies in apical positions of CuO_5 tetragonal pyramid. $PrSrCuO_{3.69}$ shows much larger oxygen loss in comparison with $Pr_{1.6}Sr_{0.4}CuO_{3.98}$. Thus, the decrease of the oxygen stoichiometry index (Δδ) in air at 298–1173 K for $PrSrCuO_{3.69}$ and $Pr_{1.6}Sr_{0.4}CuO_{3.98}$ is ~0.11 and ~0.05, respectively. Such behavior may be explained by higher amounts of Cu^{3+} being unstable at high temperatures in the T-phase in comparison with the T*-phase. From XAS data it has been concluded that oxidation state of praseodymium is +3 in Pr_2CuO_4 and $PrSrCuO_{3.69}$, while $Pr_{1.6}Sr_{0.4}CuO_{3.98}$ contains ~30% of Pr^{4+} [10,13]. Therefore the formal oxidation state of copper is ~+2 in Pr_2CuO_4 and $Pr_{1.6}Sr_{0.4}CuO_{3.98}$ and ~+2.4 in $PrSrCuO_{3.69}$.

3.2. High-temperature thermal expansion behavior of $Pr_{2-x}Sr_xCuO_{4-\delta}$

Thermal expansion curves in air for $Pr_{2-x}Sr_xCuO_{4-\delta}$ (x = 0.0, 0.4, 1.0) are given in Fig. 3; calculated thermal expansion coefficients (TECs) are presented in Table 1. Pr_2CuO_4 expands nearly linear and shows the lowest TEC of 11.8 ppm K^{-1} among studied compositions. For $PrSrCuO_{3.69}$ and $Pr_{1.6}Sr_{0.4}CuO_{3.98}$ two regions with different TEC values are observed: low- (up to ~773 K) and high-temperature ones (773–1273 K). They are results of the chemical expansion, which occurs due to the decrease of oxygen content with temperature (Fig. 2). However, the thermal expansion of $PrSrCuO_{3.69}$ and $Pr_{1.6}Sr_{0.4}CuO_{3.98}$ demonstrates a completely different behavior. For $Pr_{1.6}Sr_{0.4}CuO_{3.98}$ the TEC at the high-temperature range is higher in comparison with the low-temperature one while reverse situation is found for $PrSrCuO_{3.69}$ (see Table 1).

Temperature variation of the unit cell parameters for $PrSrCuO_{3.69}$ and $Pr_{1.6}Sr_{0.4}CuO_{3.98}$ is presented in Fig. 4a and b, respectively. TEC for individual unit cell parameters and calculated linear TEC (TEC($V^{1/3}$)) are given in Table 2. TEC values calculated from the temperature dependence of unit cell volume ($V^{1/3}$) are very close to those from dilatometry data (Table 1). Anisotropy of the thermal expansion is observed for both compounds and the TEC(a)/TEC(c) ratio for $PrSrCuO_{3.69}$ and $Pr_{1.6}Sr_{0.4}CuO_{3.98}$ in the low-temperature range is similar (0.65). This situation is opposite to what observed for undoped Pr_2CuO_4, where an anomalous anisotropy of TEC was observed with TEC(a)/TEC(c) = 1.37 [9]. It was explained by strong hybridization of Pr *f*-orbitals with appropriate O 2*p*-orbitals. Such behavior was detected only for Pr_2CuO_4 and not for other rare-earth cuprates R_2CuO_4 [9]. Apparently, partial replacement of Sr for Pr leads to the appearance of rock-salt slabs in the crystal structure and creates longer interatomic distances between A-cation and O atoms making the thermal expansion behavior of $Pr_{2-x}Sr_xCuO_4$ similar to that found for other layered compounds.

Temperature variation of the *a*-parameter of $PrSrCuO_{3.69}$ is clearly different in the low- and high-temperature ranges, while the *c*-parameter increases nearly monotonically (Fig. 4a). These temperature ranges correspond to those observed in the TG study and can be attributed to the start of oxygen elimination from the crystal structure. For $Pr_{1.6}Sr_{0.4}CuO_{3.98}$, where the oxygen loss is less pronounced (Fig. 2a), the peculiarities of the temperature dependence for *a*-parameter appeared only at T > 973 K, where an acceleration of the weight loss takes place (Fig. 4b). The temperature behavior of the *a*-parameter (TEC(a)) for $PrSrCuO_{3.69}$ is different in comparison with $Pr_{1.6}Sr_{0.4}CuO_{3.98}$. Thus, in $PrSrCuO_{3.69}$ TEC(a) decreases from 12.6 to 8.2 ppm K^{-1} with increasing temperature contrary to what found for $Pr_{1.6}Sr_{0.4}CuO_{3.98}$, where it increases from 12.6 to 18.0 ppm K^{-1} (Fig. 4a and b). This correlates with the thermal expansion behavior observed from dilatometry data (Table 1) and may be most likely explained by different distribution of oxygen vacancies in the crystal structures of $PrSrCuO_{3.69}$ and $Pr_{1.6}Sr_{0.4}CuO_{3.98}$.

Due to low accuracy in the determination of the positions, occupancies and atomic displacement parameters of oxygen atoms from XRPD

Table 1
Unit cell parameters and TECs from dilatometry data for $Pr_{2-x}Sr_xCuO_{4-\delta}$, x = 0.0, 0.3, 0.4, 1.0 and 1.3.

Composition	Type	a, Å	c, Å	TEC, ppm K^{-1}
$Pr_2CuO_{4.02\pm0.02}$	T′	3.9609 (1)	12.2210 (6)	11.8 (373–1273 K)
$Pr_{1.7}Sr_{0.3}CuO_{3.96\pm0.02}$	T*	3.8699 (1)	12.4885 (5)	12.4 (423–773 K); 15.6 (773–1273 K)
$Pr_{1.6}Sr_{0.4}CuO_{3.98\pm0.02}$	T*	3.8626 (1)	12.4876 (6)	14.9 (423–773 K); 17.3 (773–1273 K)
$PrSrCuO_{3.69\pm0.02}$	T	3.7439 (1)	12.9023 (4)	14.1 (423–773K); 13.7 (873–1273 K)
$Pr_{0.7}Sr_{1.3}CuO_{3.49\pm0.02}$	T	3.7383 (1)	12.8174 (5)	13.2 (423–843K); 14.1 (953–1273 K)

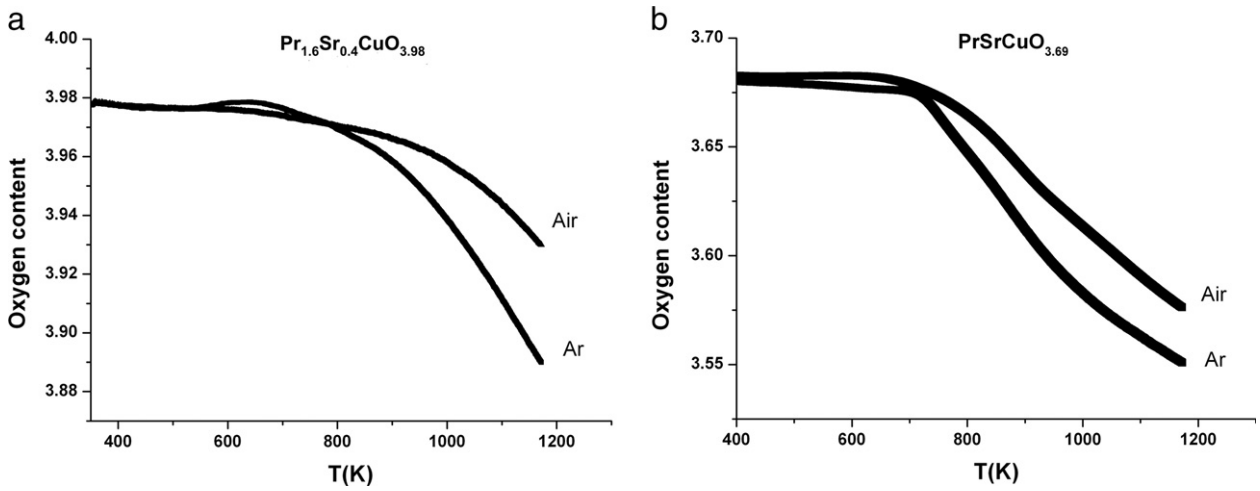

Fig. 2. Temperature dependence of the oxygen content for $Pr_{2-x}Sr_xCuO_{4-\delta}$, x = 0.4 (a) and 1.0 (b) in air and Ar as derived from TG data.

data, it is difficult to make definite conclusion about preferred site for the formation of oxygen vacancies with temperature in the crystal structures of $PrSrCuO_{3.69}$ and $Pr_{1.6}Sr_{0.4}CuO_{3.98}$. According to the crystal structure refinement of $PrSrCuO_{3.69}$ from room temperature neutron powder diffraction data [10], oxygen vacancies are localized in equatorial positions of CuO_6-octahedra (oxygen O1). Energy gain of the formation of oxygen vacancies in equatorial positions of CuO_6-octahedra in T-phases was earlier demonstrated by MD calculations for $La_{2-x}Sr_xCuO_{4-\delta}$, x = 0.37 and 1.0 [14]. One can assume that upon heating oxygen vacancies continue to form at equatorial positions and resulted in shortening of Cu – O1 in-plane bond length. This leads to a slowdown of the expansion rate of *a*-parameter with temperature, which is determined by Cu – O1 bond length. The situation is opposite for the crystal structure of $Pr_{1.6}Sr_{0.4}CuO_{3.98}$ where oxygen vacancies are most likely formed in axial position of tetragonal CuO_5 pyramid. The formation of oxygen vacancies results in the increase of copper ionic radius due to the reduction of oxidation state and leads to the increase *a*-parameter at this temperature range.

3.3. High-temperature electrical conductivity of $Pr_{2-x}Sr_xCuO_{4-\delta}$, x = 0.4, 1.0

Temperature dependences of electrical conductivity at variable oxygen partial pressure for $Pr_{1.6}Sr_{0.4}CuO_{3.98}$ and $PrSrCuO_{3.69}$ are given in Fig. 5a and b. For $Pr_{1.6}Sr_{0.4}CuO_{3.98}$ the electrical conductivity increases over the whole studied temperature range, while for

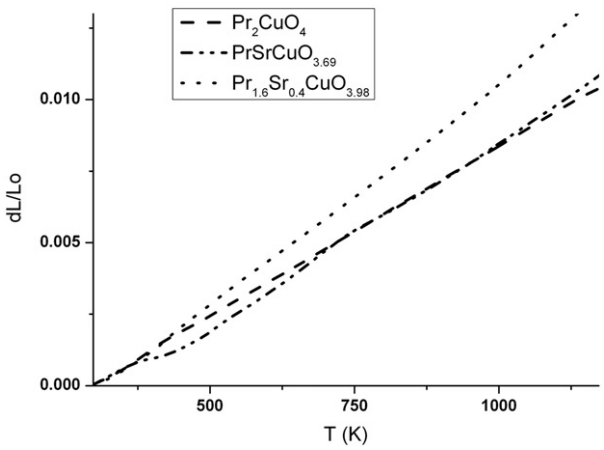

Fig. 3. Dilatometric curves for $Pr_{2-x}Sr_xCuO_{4-\delta}$ (x = 0.0; 0.4; 1.0) in air.

$PrSrCuO_{3.69}$ the decrease of conductivity takes place at T > 673 K for $p_{O_2} = 10^{-2}$–0.21 atm. This decrease is not observed at low oxygen partial pressures ($p_{O_2} = 10^{-4}$–10^{-3} atm), see Fig. 5b. Such difference in behavior of the T- and T*-phases is most likely attributed to the variation of their oxygen content as found by the TG study. As mentioned above, $PrSrCuO_{3.69}$ demonstrates much larger variation of oxygen content in comparison with $Pr_{1.6}Sr_{0.4}CuO_{3.98}$.

Temperature dependence of electrical conductivity (σ) for both compounds at T = 373–673 K can be satisfactory fitted by Arrhenius-like law modified for small polarons hopping:

$$\sigma(T) = \frac{A}{T}\exp\left(-\frac{E_a}{kT}\right), \tag{1}$$

where T is the absolute temperature, k — Boltzmann's constant, A — a pre-exponential factor, and E_a — the activation energy. Calculated values of E_a versus p_{O_2} are given in Fig. 6.

For both compounds E_a significantly increases with decreasing p_{O_2}. It should be mentioned that $PrSrCuO_{3.69}$ demonstrates lower values of E_a in comparison with $Pr_{1.6}Sr_{0.4}CuO_{3.98}$ (Fig. 6) in the whole studied oxygen partial pressure range. This can be most likely explained by a broader conduction band of $PrSrCuO_{3.69}$ due to shorter in-plane Cu-O distances, see *a*-parameter in Table 1.

The increase of electrical conductivity and decrease of E_a with p_{O_2} suggest *p*-type conductivity in $Pr_{2-x}Sr_xCuO_{4-\delta}$. It can be described by a defect model similar to that found for doped La_2CuO_4 [15,16]. In cuprates the occurrence of holes is related to the presence of Cu^{3+} due to partial heterovalent substitution of R^{3+} by Sr^{2+} in R_2CuO_4. However, because of limited stability of Cu^{3+}, such replacement partially leads to the formation of oxygen vacancies ($V_O^{\bullet\bullet}$). The formation of holes ($Cu_{Cu}^{\bullet}$ or $h^{\bullet}$) can be expressed by the following quasi-chemical equation (Kröger–Vink notations) [15]:

$$2Cu_{Cu}^{x} + V_O^{\bullet\bullet} + \frac{1}{2}O_2(g) \rightarrow 2Cu_{Cu}^{\bullet} + O_O^{x}. \tag{2}$$

The formation of oxygen vacancies by partial heterovalent substitution of Pr^{3+} by Sr^{2+} is described by:

$$2SrO \xrightarrow{Pr_2O_3} 2Sr_{Pr}^{'} + 2O_O^{x} + V_O^{\bullet\bullet}, \tag{3}$$

where $Sr_{Pr}^{'}$ is the strontium atom in the regular praseodymium position, and O_O^{x} is the oxygen atom in the regular oxygen position. One can assume a higher concentration of holes in $PrSrCuO_{3.69}$ in comparison with $Pr_{1.6}Sr_{0.4}CuO_{3.98}$, due to a higher oxidation state of copper (~+2.4) as discussed earlier. However, the electrical conductivity of

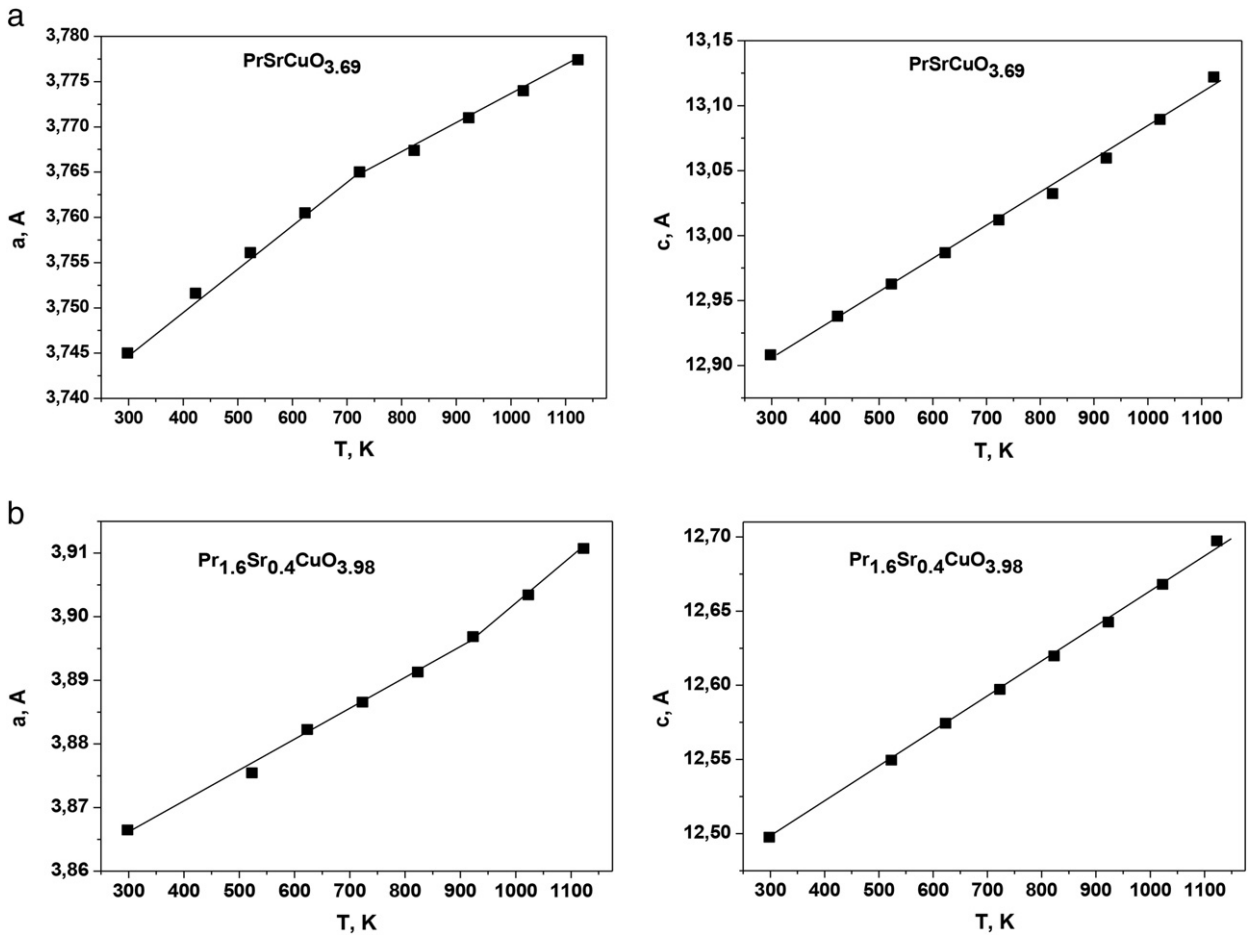

Fig. 4. Temperature variation of the unit cell parameters for $PrSrCuO_{3.69}$ (a) and $Pr_{1.6}Sr_{0.4}CuO_{3.98}$ (b).

$PrSrCuO_{3.69}$ at T < 673 K is only slightly higher in comparison with $Pr_{1.6}Sr_{0.4}CuO_{3.98}$ (σ(453 K, p_{O_2} = 0.21 atm) = 12.2 S/cm and 11.1 S/cm for $PrSrCuO_{3.69}$ and $Pr_{1.6}Sr_{0.4}CuO_{3.98}$, respectively). At T > 673 K the conductivity of $PrSrCuO_{3.69}$ starts to decrease and becomes significantly lower in comparison with $Pr_{1.6}Sr_{0.4}CuO_{3.98}$ (σ(993 K, p_{O_2} = 0.21 atm) = 34 S/cm and 7 S/cm for $Pr_{1.6}Sr_{0.4}CuO_{3.98}$ and $PrSrCuO_{3.69}$, respectively). A decrease of conductivity for $PrSrCuO_{3.69}$ with temperature is most likely associated with the formation of oxygen vacancies in equatorial positions of CuO_6 octahedra in the crystal structure of this cuprate, as discussed in the previous section. One can assume that the formation of oxygen vacancies in T-phase leads to the decrease of holes concentration and also to the difficulties of small polaron hopping between two adjacent Cu cations and to decrease of polaron mobility.

Additional information about the nature of charge carriers can be extracted from the analysis of the conductivity dependences on oxygen partial pressure at fixed temperature. The isotherms lg(σ)–lg(p_{O_2}) are essentially linear for both compounds (Fig. 7a and b). For $PrSrCuO_{3.69}$ the slope of lg(σ)–lg(p_{O_2}) approaches ~1/4 with increasing temperature (Fig. 7a). Such behavior ($\sigma \propto p_{O_2}^{\frac{1}{4}}$) can be described by a model similar to that for $La_{2-x}Sr_xCuO_{4-\delta}$ [16]. In this case Eq. (2) can be re-written as:

$$\frac{1}{2}O_2(g) + V_O^{\bullet\bullet} \Leftrightarrow O_O^x + 2h^{\bullet} \tag{4}$$

with equilibrium constant (K_{ox}) defined as:

$$K_{ox} = \frac{[h^{\bullet}]^2 [O_O^x]}{p_{O_2}^{\frac{1}{2}} [V_O^{\bullet\bullet}]}. \tag{5}$$

At high Sr^{2+} content charge neutrality requirement can be expressed as:

$$\left[Sr'_{Pr}\right] = 2[V_O^{\bullet\bullet}] + [h^{\bullet}]. \tag{6}$$

At high concentration of oxygen vacancies as in the case of $PrSrCuO_{3.69}$, it can be re-written as:

$$\left[Sr'_{Pr}\right] = 2[V_O^{\bullet\bullet}] >> [h^{\bullet}]. \tag{7}$$

Combination of Eqs. (5) and (7) resulted in the following dependence of the hole concentration on oxygen partial pressure:

$$[h^{\bullet}] = \left(K_{ox} \cdot \frac{\left[Sr'_{Pr}\right]}{2[O_O^x]}\right)^{\frac{1}{2}} \cdot p_{O_2}^{\frac{1}{4}} \quad \text{or} \quad \sigma \propto [h^{\bullet}] \propto p_{O_2}^{\frac{1}{4}}. \tag{8}$$

Table 2
Thermal expansion coefficients (TEC) (in ppm K^{-1}) of $PrSrCuO_{3.69}$ and $Pr_{1.6}Sr_{0.4}CuO_{3.98}$ from HT XRPD (TEC($V^{1/3}$)) together with TEC for the individual unit cell parameters.

Compound	TEC (a), ppm K^{-1}	TEC (c), ppm K^{-1}	TEC ($V^{1/3}$), ppm K^{-1}
$PrSrCuO_{3.69}$ (T)	12.6 (298–723 K) 8.8 (823–1123 K)	20.0 (298–1123 K)	14.6 (298–723 K) 13.5 (823–1123 K)
$Pr_{1.6}Sr_{0.4}CuO_{3.98}$ (T*)	12.6 (298–923 K) 17.7 (923–1123 K)	19.4 (298–1123 K)	14.6 (298–923 K) 19.1 (923–1123 K)

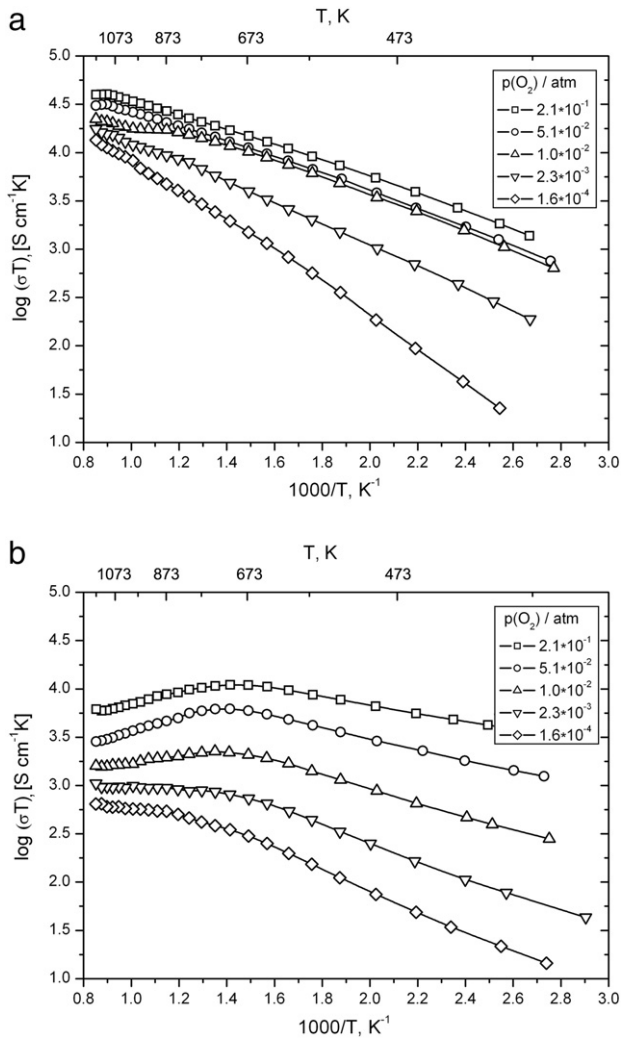

Fig. 5. Temperature dependences of electrical conductivity in $Pr_{1.6}Sr_{0.4}CuO_{3.98}$ (a) and $PrSrCuO_{3.69}$ (b) at variable oxygen partial pressure.

For $Pr_{1.6}Sr_{0.4}CuO_{3.98}$ the slope of $\lg(\sigma)$–$\lg(p_{O_2})$ decreases down to ~1/6 with increasing temperature (Fig. 7b). Such dependence ($\sigma \propto p_{O_2}^{\frac{1}{6}}$) is typical for the process of insertion of oxygen atoms into interstitial

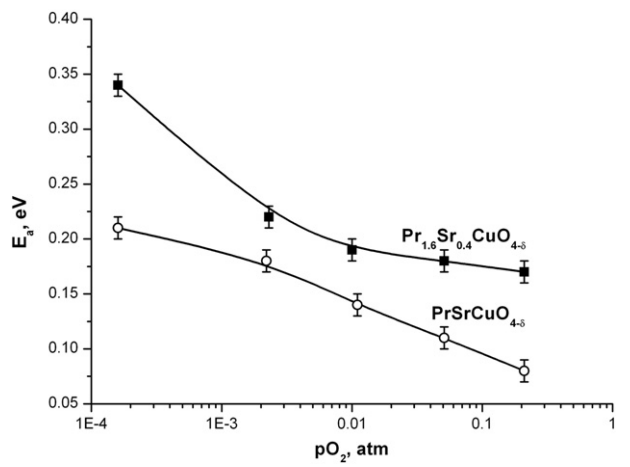

Fig. 6. Oxygen partial pressure (p_{O_2}) dependences of activation energies (E_a) for $Pr_{1.6}Sr_{0.4}CuO_{3.98}$ and $PrSrCuO_{3.69}$ at 373–673 K (lines are guides for eyes only).

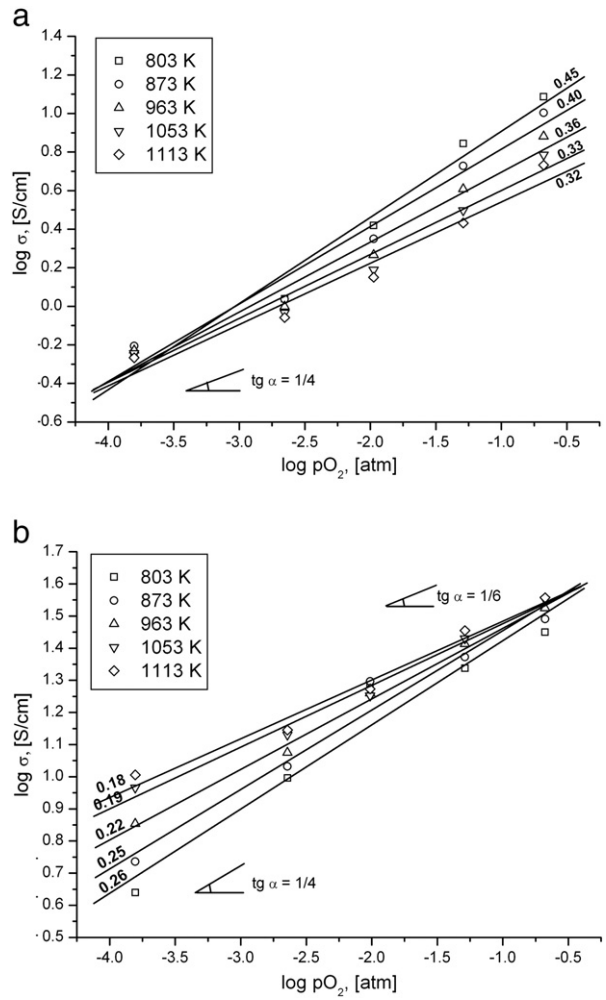

Fig. 7. Dependence of the conductivity in $PrSrCuO_{3.69}$ (a) and $Pr_{1.6}Sr_{0.4}CuO_{3.98}$ (b) on oxygen partial pressure (digits designate the slope of corresponding help lines).

positions in a crystal structure and can be expressed by the following quasi-chemical equation:

$$\frac{1}{2}O_2(g) \Leftrightarrow O_i'' + 2h^{\bullet} \tag{9}$$

where O_i'' is the oxygen atom at interstitial position. The equilibrium constant (K_{ox}) for this reaction is:

$$K_{ox} = \frac{\left[O_i''\right]\left[h^{\bullet}\right]^2}{p_{O_2}^{\frac{1}{2}}}. \tag{10}$$

Taking into account the electroneutrality requirement ($[h^{\bullet}] = 2[O_i'']$), the concentration of holes or conductivity on the oxygen partial pressure can be expressed as:

$$\left[h^{\bullet}\right] = (2K_{ox})^{\frac{1}{3}} \cdot p_{O_2}^{\frac{1}{6}} \quad \text{or} \quad \sigma \propto \left[h^{\bullet}\right] \propto p_{O_2}^{\frac{1}{6}}. \tag{11}$$

Such behavior was also observed for undoped La_2CuO_4 [17] and $La_2Cu_{0.5}Ni_{0.5}O_{4+\delta}$ [18]. In the latter case it was explained by the interaction of charge carriers resulted in non-applicability of the ideal solution model.

In summary, although both $Pr_{1.6}Sr_{0.4}CuO_{3.98}$ and $PrSrCuO_{3.69}$ show quite similar values of electrical conductivity, which both are substantially lower in comparison with Pr_2CuO_4, they demonstrate different temperature and p_{O_2} dependences of conductivity (Figs. 5 and 7). The

decrease of conductivity with temperature found for $PrSrCuO_{3.69}$ can be explained by a larger variation in oxygen content with temperature of this phase in comparison with $Pr_{1.6}Sr_{0.4}CuO_{3.98}$. The compounds demonstrate different mechanisms of the formation of charge carries (holes) as can be seen from the slopes of $\lg(\sigma)$–$\lg(p_{O_2})$ curves (Fig. 7). While for $PrSrCuO_{3.69}$ the formation of holes occurs mainly by the mechanism of oxygen insertion into vacant regular positions (Eq. (4)) in the whole high-temperature range, for $Pr_{1.6}Sr_{0.4}CuO_{3.98}$ such behavior can be observed at low temperature only. At high temperatures the generation of charge carriers in $Pr_{1.6}Sr_{0.4}CuO_{3.98}$ is due to insertion of oxygen into interstitial positions (Eq. (9)).

3.4. Oxygen diffusion in $Pr_{1.6}Sr_{0.4}CuO_{3.98}$

The oxygen tracer diffusion coefficient D_T and the surface exchange coefficient k for $Pr_{1.6}Sr_{0.4}CuO_{3.98}$ were determined by the isotopic exchange depth profile (IEDP) technique using SIMS after isotopic exchange of ^{16}O for ^{18}O in the ceramic samples. As an example, the ^{18}O isotopic concentration depth profile of $Pr_{1.6}Sr_{0.4}CuO_{3.98}$ annealed at 1073 K is given in Fig. 8. The oxygen tracer diffusion (D_T) and surface exchange (k) coefficients were determined by non-linear least squares regression based on fitting of the diffusion profiles using the Crank relation, solution of the Fick's second law of the diffusion, similar to the procedure described in references [19,20]. Calculated values of D_T and k are given in Table 3. Dependences of bulk oxygen tracer diffusion and surface exchange coefficients on reverse temperature are given in Fig. 9. They can be satisfactory fitted by the Arrhenius law with activation energies (E_a) for oxygen tracer diffusion and surface exchange coefficients being 175 ± 15 kJ mol^{-1} (1.81 eV) and 85 ± 3 kJ mol^{-1} (0.88 eV), respectively.

Selected data on oxygen tracer diffusion and surface exchange coefficients as determined by SIMS on polycrystalline samples of various layered cuprates and nickelates are summarized in Table 4. With an exception of La_2CuO_4, cuprates show lower values of oxygen diffusion and surface exchange coefficients in comparison with corresponding nickelates. The most plausible reason for such behavior is already mentioned above compressed fluorite slab in the crystal structures of R_2CuO_4, R = Pr–Gd with T′-structure in comparison with T-structure. Partial substitution of Pr by Sr as in $Pr_{1.6}Sr_{0.4}CuO_{3.98}$ leads to the increase of oxygen tracer diffusion coefficient by 3 orders of magnitude and resulted in substantial decrease of activation energy for oxygen tracer diffusion coefficient from 290 ± 28 kJ mol^{-1} for Pr_2CuO_4 [9] to 175 ± 15 kJ mol^{-1} for $Pr_{1.6}Sr_{0.4}CuO_{3.98}$. At the same time, activation energy for surface exchange coefficient for $Pr_{1.6}Sr_{0.4}CuO_{3.98}$ drops by more than two times down to 85 ± 3 kJ mol^{-1} from 197 ± 28 kJ mol^{-1} observed in Pr_2CuO_4. The possible explanation for this is the appearance of weakly bounded apical oxygen atom in the crystal structure of $Pr_{1.6}Sr_{0.4}CuO_{3.98}$, which facilitates the creation of oxygen vacancies, in comparison with non-anion deficient Pr_2CuO_4. Both values of D_T and E_a for $Pr_{1.6}Sr_{0.4}CuO_{3.98}$ are within the same range as for perovskite-related oxides with high oxide-ion conductivity like cobaltites and nickelates. It should be mentioned that contrary result is obtained for Sr substituted La_2CuO_4 where oxygen diffusion decreases with increasing amount of strontium [22,23]. Observed changes in oxygen diffusion of $Pr_{1.6}Sr_{0.4}CuO_{3.98}$ may be explained by the appearance of rock-salt slab in the crystal structure of T*-phase. In contrast to fluorite slab, the presence of rock-salt slab gives a chance for the development of oxygen vacancies and creates the room for the diffusion of oxygen. Thickness of the rock-salt and fluorite slabs in the crystal structure of $Pr_{1.6}Sr_{0.4}CuO_{3.98}$ are 2.78 Å and 2.59 Å [10], respectively. This indicates more space for diffusion of oxygen in the rock-salt slab in comparison with fluorite one. It should be mentioned that the thickness of fluorite slab in the crystal structure of $Pr_{1.6}Sr_{0.4}CuO_{3.98}$ is larger in comparison with undoped Pr_2CuO_4 (2.48 Å) making additional diffusion of oxygen through this slab more likely.

Table 3
Calculated values of D_T and k for $Pr_{1.6}Sr_{0.4}CuO_{3.98}$ at various temperatures.

T, K	D_T, cm^2/s	k, cm/s
973	6.7×10^{-10}	7.7×10^{-8}
1073	8.1×10^{-9}	1.9×10^{-7}
1173	3.3×10^{-8}	4.4×10^{-7}
1223	5.7×10^{-8}	6.7×10^{-7}

4. Conclusion

High temperature properties of $Pr_{2-x}Sr_xCuO_{4-\delta}$ show large correlation with their crystal structures. Thus, layered cuprates represent excellent model system for studying interplay between the crystal structure and properties of layered perovskite-related oxides important for use in high-temperature electrochemical devices like TEC, electronic and oxide-ion conductivities.

Strong interactions in T′-phase resulted in temperature independent oxygen content and lower TEC value due to the absence of chemical expansion. In the crystal structure of $Pr_{1.6}Sr_{0.4}CuO_{3.98}$ oxygen vacancies are most likely localized in the axial position of CuO_5 square pyramid belonging to rock-salt slab and increasing of temperature resulted in an elongation of Cu – O equatorial bonds due partial reduction of the

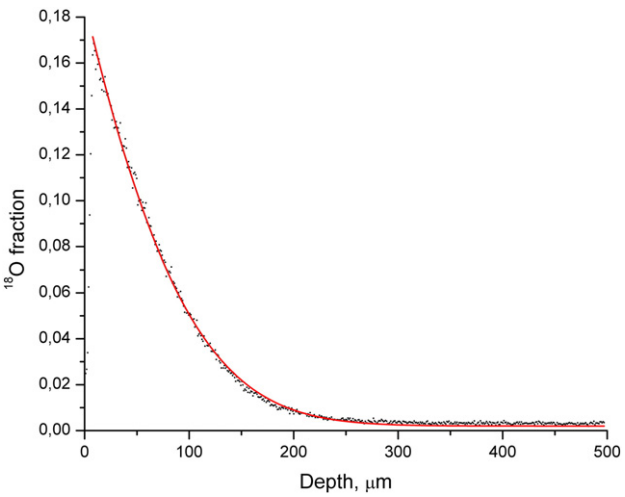

Fig. 8. ^{18}O penetration profile determined for $Pr_{1.6}Sr_{0.4}CuO_{3.98}$ at 1073 K. The points refer to experimental points and curve for the fitting results.

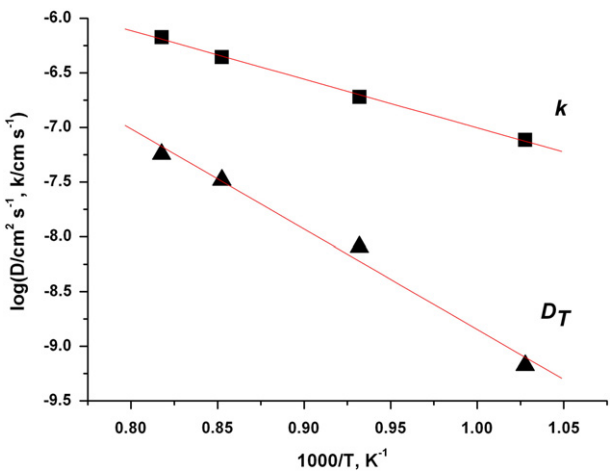

Fig. 9. Bulk oxygen tracer diffusion (D_T) and surface exchange (k) coefficients obtained for $Pr_{1.6}Sr_{0.4}CuO_{3.98}$ as a function of inverse temperature. Squares refer to surface exchange, triangles to oxygen tracer diffusion coefficients.

Table 4
Oxygen tracer diffusion and surface exchange coefficients determined by SIMS on the polycrystalline samples of selected layered cuprates and nickelates.

Compound	Structure	D_T, cm^2/s	k, cm/s	T, K	Ref.
Pr_2NiO_4	T	4.0×10^{-8}	5.0×10^{-7}	923	[21]
La_2CuO_4	T	~10^{-8}	~10^{-6}	973	[3]
Pr_2CuO_4	T′	7.2×10^{-13}	1.2×10^{-8}	973	[9]
$Pr_{1.6}Sr_{0.4}CuO_{3.98}$	T*	6.7×10^{-10}	7.7×10^{-8}	973	Present study

oxidation state of Cu. In contrast, the localization of oxygen vacancies in equatorial positions of CuO_6 octahedra in $PrSrCuO_{3.69}$ with T-structure causes shortening of the average equatorial Cu – O bonds and results in the decrease of TEC at high temperature. Such behavior is not common for oxygen-deficient oxides where normally increasing of temperature resulted in chemical expansion.

Together with the ability to form oxygen vacancies in $Pr_{1.6}Sr_{0.4}CuO_{3.98}$, the appearance of rock-salt slab in the crystal structure of T*-phase leads to the extension of room for the fast diffusion of oxygen. This resulted in much higher values of oxygen diffusion in T*-phase in comparison with that in T′-phase. Thus, obtained results demonstrate the importance of the presence of rock-salt slab in the crystal structure of layered perovskite-related R_2MO_4 oxides for fast oxygen diffusion. On the other hand, the presence of fluorite slab creates conditions for lower TEC due minimized chemical expansion.

Acknowledgments

This work was partially supported by the Ministry of Science and Education of Russian Federation (state contract 14.740.12.1358), Russian Foundation for Basic Research (grant nos. 14-08-01260 and 14-03-01083), and MSU-Development Program up to 2020.

References

[1] B.C.H. Steele, J. Mater. Sci. 36 (2001) 1053–1068.
[2] S.B. Adler, Chem. Rev. 104 (2004) 4791–4843.
[3] E. Boehm, J.-M. Bassat, M.C. Steil, P. Dordor, F. Mauvy, J.-C. Grenier, Solid State Sci. 5 (2003) 973–981.
[4] A. George, I. Gopalakrishnan, M. Karkhanavala, Mater. Res. Bull. 9 (1974) 721–726.
[5] K. Zheng, A. Gorzkowska-Sobas, K. Swierczek, Mater. Res. Bull. 47 (2012) 4089–4095.
[6] A. Chroneos, D. Parfitt, J.A. Kilner, R.W. Grimes, J. Mater. Chem. 20 (2010) 266–270.
[7] G.N. Mazo, Yu.A. Mamaev, M.Z. Galin, M.S. Kaluzhskikh, A.K. Ivanov-Schitz, Inorg. Mater. 47 (2011) 1218–1226.
[8] N.V. Lyskov, M.S. Kaluzhskikh, L.S. Leonova, G.N. Mazo, S.Ya. Istomin, E.V. Antipov, Int. J. Hydrogen Energy 37 (2012) 18357–18364.
[9] M.S. Kaluzhskikh, S.M. Kazakov, G.N. Mazo, S.Ya. Istomin, E.V. Antipov, A.A. Gippius, Yu Fedotov, S.I. Bredikhin, Yi Liu, G. Svensson, Z. Shen, J. Solid State Chem. 184 (2011) 698–704.
[10] H.Y. Hwang, S.-W. Cheong, A.S. Cooper, L.W. Rupp Jr., B. Batlogg, G.H. Kwei, Z. Tan, Physica C 192 (1992) 362–371.
[11] J.-C. Grivel, N.H. Andersen, J. Alloys Compd. 436 (2007) 261–265.
[12] J. Gopalakrishnan, M. Subramanian, C.C. Torardi, J.P. Attfield, A.W. Sleight, Mater. Res. Bull. 24 (1989) 321–330.
[13] Zhengquan Tan, S.M. Heald, S.-W. Cheong, A.S. Cooper, J.I. Budnick, Phys. Rev. B 45 (1992) 2593–2596.
[14] G.N. Mazo, S.N. Savvin, Solid State Ionics 175 (2004) 371–374.
[15] L. Shen, P. Salvador, T.O. Mason, K. Fueki, J. Phys. Chem. Solids 57 (1996) 1977–1987.
[16] D.J.L. Hong, D.M. Smyth, J. Solid State Chem. 102 (1993) 250–260.
[17] D.J.L. Hong, D.M. Smyth, J. Solid State Chem. 97 (1992) 427–433.
[18] F. Mauvy, J.M. Bassat, E. Boehm, P. Dordor, J.P. Loup, Solid State Ionics 158 (2003) 395–407.
[19] J.A. Kilner, S.J. Skinner, H.H. Brongersma, J. Solid State Electrochem. 15 (2011) 861–876.
[20] A. Kilner, R.A. De Souza, I.C. Fullarton, Solid State Ionics 86–88 (1996) 703–709.
[21] E. Boehm, J.-M. Bassat, P. Dordor, F. Mauvy, J.-C. Grenier, Ph. Stevens, Solid State Ionics 176 (2005) 2717–2725.
[22] E.J. Opila, H.L. Tuller, B.J. Wuensch, J. Maier, J. Am. Ceram. Soc. 76 (1993) 2363–2369.
[23] J. Claus, G. Borchardt, S. Weber, J.-M. Hiver, S. Scherrer, Mater. Sci. Eng. B 38 (1996) 251–257.